Nanoscale

COMMUNICATION

View Article Online
View Journal | View Issue

Cite this: *Nanoscale*, 2019, **11**, 23126

Received 11th October 2019,
Accepted 8th November 2019

DOI: 10.1039/c9nr08753b

rsc.li/nanoscale

2D MoS_2 nanosheets on 1D anodic TiO_2 nanotube layers: an efficient co-catalyst for liquid and gas phase photocatalysis†

Martin Motola, [a] Michal Baudys, [b] Raul Zazpe, [a,c] Miloš Krbal, [a] Jan Michalička, [c] Jhonatan Rodriguez-Pereira, [a] David Pavliňák, [d] Jan Přikryl, [a] Luděk Hromádko, [a,c] Hanna Sopha, [a,c] Josef Krýsa [b] and Jan M. Macak *[a,c]

One-dimensional TiO_2 nanotube layers with different dimensions were homogeneously decorated with 2D MoS_2 nanosheets *via* atomic layer deposition and employed for liquid and gas phase photocatalysis. The 2D MoS_2 nanosheets revealed a high amount of exposed active edge sites and strongly enhanced the photocatalytic performance of TiO_2 nanotube layers.

Self-organized TiO_2 nanotube (TNT) layers, prepared *via* electrochemical anodization,[1–3] represent unique one-dimensional (1D) nanomaterials. TNT layers are commonly accepted to be excellent for photoelectrochemical applications, in particular photocatalysis.[1–4] Their unique geometry and properties, such as a high surface area, tunability of dimensions, and strong light absorption, are their main advantages over other TiO_2 nanostructures.[5–9] The photocatalysis on TiO_2 surfaces is based on UV light absorption, generation of e^-/h^+ pairs, and formation of radicals with high oxidizing power that subsequently decompose organic matter.[4,5] Due to the band gap of ~3.2 eV for anatase TiO_2, a photoresponse can only be generated by UV light irradiation.[10–12]

In recent years, 2D transition metal dichalcogenides, especially MoS_2, have attracted considerable attention owing to their suitable band gap for VIS light absorption, high carrier mobility and relatively good stability against photocorrosion.[13,14] Structurally, MoS_2 is composed of covalently bound S–Mo–S stacks held together by weak van der Waals interactions determining the 2D nature of the crystalline phases.[15] Bulk MoS_2 has an indirect band gap of ~1.3 eV which increases, due to quantum confinement effects, to ~1.9 eV for monolayer sheets.[16,17] Approximately 25% of edge sites are active for the photocatalytic reaction.[18] All in all, mono- and few-layered sheets of MoS_2 exhibit a range of intriguing properties, absent in the bulk.

The intimate contact between TiO_2 and MoS_2 results into a type-II heterojunction structure with favorable positions of conduction and valence bands in the energy diagram.[13] The photogenerated e^- from the valence band of MoS_2 are directly transferred to its conduction band, leaving the newly created h^+ in the valence band of MoS_2. As the conduction band potential of TiO_2 is lower compared to that of MoS_2, TiO_2 acts as an electron acceptor of the photogenerated e^- from the conduction band of MoS_2.[19] Moreover, the e^- are trapped by oxygen molecules in the aqueous solution to form singlet oxygen.[20] Simultaneously, the photogenerated h^+ are captured within MoS_2, effectively suppressing the recombination rate of charge carriers, thus improving the photocatalytic activity.[21] The h^+ reacts with either H_2O or OH^- adsorbed onto the TiO_2 surface to produce $^{\bullet}OH$, and the e^- react with O_2 to form $^{\bullet}O_2^-$.[22] Consequently, both $^{\bullet}OH$ and $^{\bullet}O_2^-$ radicals decompose various organic pollutants to CO_2 and H_2O.[22]

So far, many methods have been explored to decorate TiO_2 materials by MoS_2, such as sputtering,[16] hydrothermal,[23,24] photoassisted electrodeposition,[24] solvothermal,[25] sol–gel,[26,27] chemical vapor deposition,[28] exfoliation,[29,30] photocatalytic reduction of $(NH_4)_2MoS_4$ to MoS_2,[31] and liquid ultrasonic mixing.[32] However, none of the above-mentioned techniques is suitable for the decoration of 1D TNT layers, as only very inhomogeneous decoration by MoS_2 nanosheets of these layers throughout their volume can be achieved. Atomic layer deposition (ALD) is the most suitable method for homogeneous decoration and coating of various 1D nanomaterials, including TNTs.[33,34] ALD is based on sequential self-limited adsorption of vapors of compatible precursors on surfaces which allows conformity all over the surface with controllable thickness at the atomic level.[33]

[a]*Center of Materials and Nanotechnologies, Faculty of Chemical Technology, University of Pardubice, Nam. Cs. Legii 565, 53002 Pardubice, Czech Republic. E-mail: jan.macak@upce.cz*
[b]*Department of Inorganic Technology, University of Chemistry and Technology Prague, Technicka 5, 16628 Prague, Czech Republic*
[c]*Central European Institute of Technology, Brno University of Technology, Purkynova 123, 61200 Brno, Czech Republic*
[d]*Department of Physical Electronics, Masaryk University, Kotlarska 2, 61137 Brno, Czech Republic*

†Electronic supplementary information (ESI) available: Experimental procedures, SEM and STEM HAAD characterization of the materials, photocurrents, Kubelka–Munk curves, XPS, XRD, micro-Raman and details of hexane photodegradation. See DOI: 10.1039/c9nr08753b

2D MoS_2 nanosheets grown on wider band gap semiconductors (*e.g.* TiO_2) serve as a sensitizer and enable enhanced production of hydrogen[16,35–37] and photodegradation of organic pollutants.[38,39] Although the photocatalysis of MoS_2 decorated TNT layers is reported,[16,24,31,40–42] all publications show inhomogeneous decoration of TNT layers with thickness >1 μm. Only TNT layers with thickness <1 μm were homogeneously decorated.[31,40,42] Furthermore, these publications focus mainly on hydrogen evolution. Only a few publications focus on the photodegradation of pollutants,[24,41,43,44] however, solely in the liquid phase. No publications focus on the photocatalytic activity of these layers in the gas phase.

In the present work, liquid (*i.e.* using a model organic dye) and gas phase (*i.e.* hexane-to-CO_2 conversion) photocatalyses are reported for TNT layers homogenously decorated by MoS_2 nanosheets. ALD was used for the homogeneous decoration of TNT layers with different dimensions using a recently described process.[45]

Fig. 1A–D show representative top-view and cross-sectional view scanning electron microscopy (SEM) images of TNT layers. ~5 μm thick TNT layers with an inner tube diameter of ~230 nm on a 2.25 cm^2 area were used for liquid phase photocatalysis (Fig. 1A and B). For gas phase photocatalysis (Fig. 1C and D), TNT layers with a thickness of ~1 μm and an inner diameter of ~45 nm on a 50 cm^2 area were used. Both types of TNT layers have a very similar aspect ratio of approx. 22. The reason for using different types of TNT layers for gas phase photocatalysis is two-fold: (i) the available gas phase setup requires the use of 50 cm^2 areas, and (ii) technological difficulties in growing 5 μm thick nanotube layers with the same (or at least similar) inner diameter nanotubes, as on the lab scale.[46,47] Details are discussed in the ESI.† Nevertheless, we achieved uniform, well adhering and crack-free TNT layers for both types of samples (ESI, Fig. S1†).

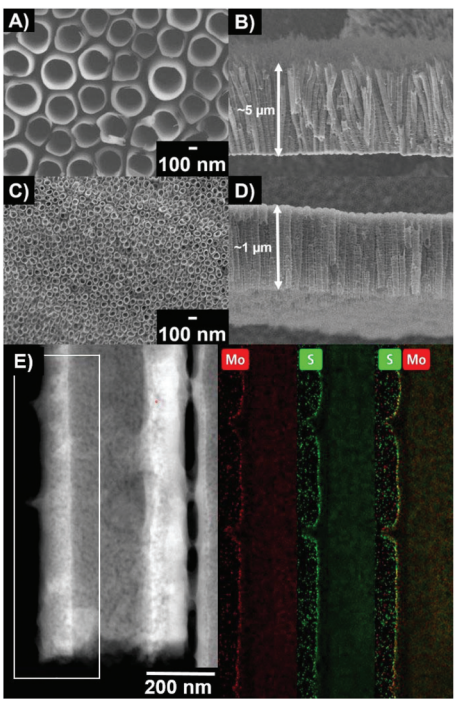

Fig. 1 SEM images of the as-prepared TiO_2 nanotube (TNT) layers: (A, C) top-view, and (B, D) cross-sectional view of 5 μm and 1 μm thick TNT layers. (E) STEM HAAD image and the corresponding STEM EDX elemental maps (obtained from the marked region) show the decoration of Mo and S species on the TNT wall and reveal a homogeneous MoS_2 decoration along the TNT wall after 2 MoS_2 ALD cycles.

For the purpose of comparison, we used TNT layers with 3 different ALD MoS_2 cycles: 1, 2 and 5. After the ALD of MoS_2, it was possible to observe MoS_2 ultrathin nanosheets on TNT layers only by TEM (not SEM), due to their extremely small dimensions. Fig. 1E shows a representative STEM HAAD image and the corresponding STEM EDX elemental maps of the chemical distribution of Mo and S elements on the fragment of a nanotube wall in the cross-sectional view after 2 MoS_2 ALD cycles. This homogeneous decoration of TNT layers with MoS_2 nanosheets was revealed over their entire volume. X-ray diffraction (XRD), micro-Raman spectroscopy (mRS) and X-ray photoelectron spectroscopy (XPS) were carried out to obtain additional information on the crystalline structure and composition (all in the ESI†). While XRD measurements could be carried out on TNT layers, mRS and XPS could be, due to the nature of these techniques and optimal signal-to-noise ratio, carried out only on planar Si wafers (ALD decorated in parallel with the TNT layers). The native SiO_2 thin layer on the Si wafer was not removed before ALD decoration. From XRD patterns (Fig. S2†), only diffractions of TiO_2 anatase and diffractions of Ti from the underlying Ti substrate were identified for blank TNT layers. In all MoS_2 decorated TNT layers, additional diffraction of MoS_2 at a 2θ of ~14.3° is visible (26622-ICSD).[45] This clearly shows the successful growth of crystalline MoS_2 nanosheets during the ALD process. Nevertheless, several peaks are observed stemming from the nonstoichiometric Mo_XS_Y compositions. The presence of MoS_2 is further confirmed by mRS (Fig. S3†). Signals at ~384 cm^{-1} and ~403 cm^{-1} which correspond to the E_{2g}^1 and A_{1g} modes of MoS_2, respectively, are observed (discussed in detail in the ESI†) when decorated by 5c MoS_2.[48] The obtained Raman spectra did not show any signal for 1c and 2c MoS_2 due to the extremely small dimensions of the nanosheets. Only signals from the underlying substrate were observed. Nevertheless, the presence of MoS_2 is confirmed by XPS for all ALD cycles (Fig. S4†). The high resolution spectra of Mo 3d show a doublet with the Mo $3d_{5/2}$ peak at 229.4 eV corresponding to the Mo^{4+} oxidation state and S 2p spectra show a doublet with the S $2p_{3/2}$ peak at 162.2 eV corresponding to the S^{2-} oxidation state. The determined S/Mo ratios are 2.03, 2.13 and 2.31 for 1c, 2c and 5c MoS_2, respectively. The doublet shape of Mo 3d is wider compared to that of pure MoS_2.[45] This is due to the presence of an additional Mo^{6+} oxidation state in the form of MoO_3, which can have a two-fold origin. Either it is the result of a partial oxidation of Mo species following the ALD process or it stems from the reaction with the O species (in the TiO_2 and SiO_2) present on the interface between substrates and the decorated MoS_2 nanosheets. Moreover, the decrease in O 1s peaks

reflects the increasing amount of S–Mo–S stacks within nanosheets. The signal intensity follows the order 1 > 2 > 5 MoS_2 ALD cycles (from the most intense to less intense).

The photoelectrochemical characteristics were recorded for blank and MoS_2 decorated 5 μm thick TNT layers in the wavelength range from 310 nm to 800 nm, as shown in Fig. 2 and the ESI (Fig. S5†). The extension of the photocurrent responses into the visible spectral region relative to the blank TNT layers is observed for all TNT layers decorated with MoS_2 nanosheets. Incident photon-to-electron conversion efficiency (IPCE, Fig. 2A) values were doubled for TNT layers with 1 and 2 MoS_2 cycles, reaching ~40%, in comparison with the blank TNT layer in the wavelength range of 350–370 nm. Due to the band gap of TiO_2 of ~3.2 eV there is no response in the VIS spectral region for blank TNT layers. In the wavelength range of 410–430 nm, the IPCE values reached ~20% for TNT layers with 1 and 2 MoS_2 cycles and about ~10% for TNTs + 5c MoS_2. This clearly shows a stronger ability of MoS_2 decorated TNT layers to produce charge carriers and more separated e^- compared to the blank layers. Also the annihilation of TiO_2 surface states by MoS_2 nanosheets might come into play, as shown previously.[37] To examine the photoresponse of TNT layers over a range of wavelengths, the photocurrent transients were recorded at a fixed bias of +0.4 $V_{vs.\ Ag/AgCl}$ with light on/off for 10 s period in the UV (Fig. 2B) and VIS spectral range (Fig. 2C). The MoS_2 decorated TNT layers show a good photocurrent switching performance with a fast response time. The type-II heterojunction interface of the MoS_2 (with a direct band gap)/TiO_2 heterostructure and also the TiO_2 surface state annihilation are responsible for such an enhancement.[4,34,40] In contrast, an increased thickness of MoS_2 nanosheets (*i.e.* theoretically 5 ALD cycles correspond to 5 S–Mo–S stacks with an indirect band gap) decreased the photoresponse in the UV spectral region compared to the blank layers. This is due to the low electron conductivity of MoS_2 that limits the e^- transfer.[44,49] Moreover, with an increased number of ALD cycles, the increasing number of S–Mo–S stacks could significantly suppress the e^- transfer in the direction perpendicular to the basal plane of the MoS_2 nanosheets.[49]

Fig. 3A and B show the photocatalytic performance (of the same TNT layers shown in Fig. 2) for the liquid phase photodegradation of methylene blue (MB) under UV and VIS irradiation, respectively. It follows a pseudo-first-order reaction.[2] Thus, its kinetics can be expressed from the linear vari-

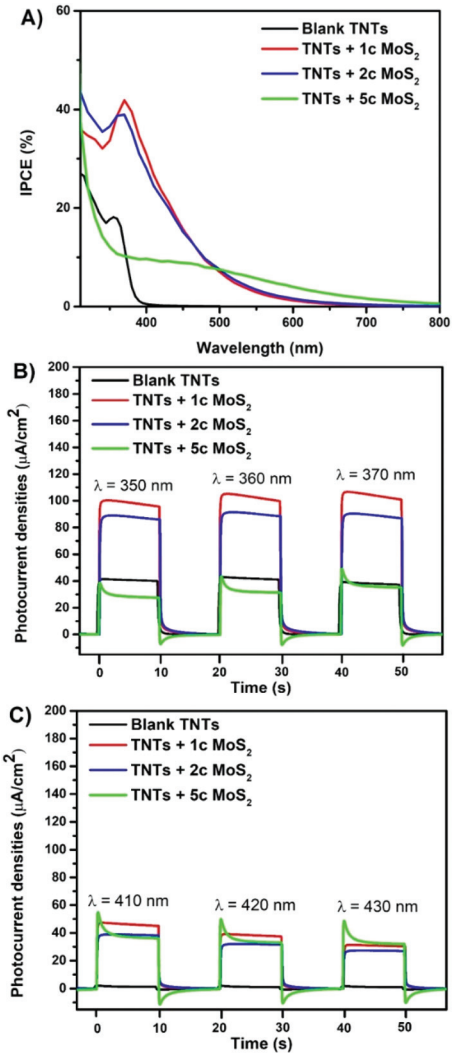

Fig. 2 (A) Incident photon-to-electron conversion efficiency (IPCE) *vs.* wavelength. Photocurrent transients recorded at (B) 350 nm, 360 nm, and 370 nm, respectively, and (C) 410 nm, 420 nm, and 430 nm, respectively, for blank, and MoS_2 decorated TNT layers. The "*Xc*" specifies the number of MoS_2 ALD cycles. All data recorded in an aqueous 0.1 M Na_2SO_4 at 0.4 $V_{vs.\ Ag/AgCl}$.

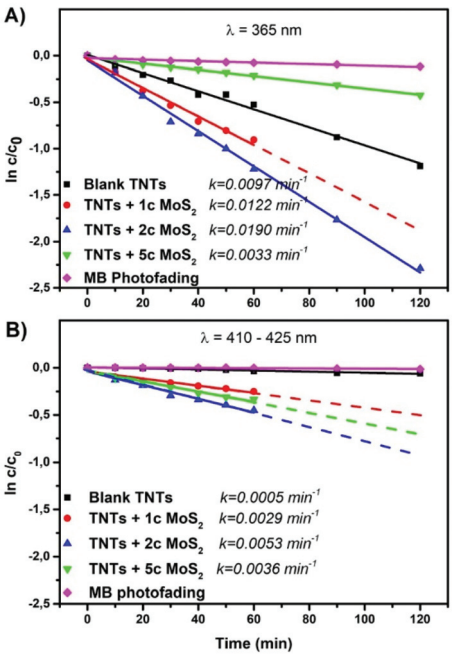

Fig. 3 Liquid phase photocatalysis: degradation rates of methylene blue (MB) for blank and MoS_2 decorated TNT layers and the resulting kinetic rate constants: (A) UV: λ = 365 nm and (B) VIS: λ = 410–425 nm. The "*Xc*" specifies the number of MoS_2 ALD cycles.

ation of ln c/c_0 as a function of time. The resulting kinetic rate constants are shown in Fig. 3.

The results clearly show that the appropriate MoS_2 decoration of TNT layers by 1 or 2 ALD cycles of MoS_2 enhances the photocatalytic activity of TNT layers. TNT layers decorated with 5 ALD MoS_2 cycles possess worse activities compared to the blank and to those with 1 or 2 cycles under UV irradiation (Fig. 3A). The band gap for this thickest MoS_2 nanosheet decoration used in here is indirect,[13,50] and it is mainly the excess of MoS_2 on the available TiO_2 surface that lowers the photocatalytic activity due to a shading effect.[51,52] This means that MoS_2 blocks the incident light absorption by TiO_2 and reduces its photoexcitation capacity. Indeed, the higher density (and shading) of MoS_2 nanosheets within TNT layers + 5c MoS_2 compared to that in TNT layers + 2c MoS_2 is clearly observed from STEM EDX (ESI, Fig. S6†). Fig. 3B shows the photodegradation of MB under VIS irradiation. Compared to the photodegradation in the UV spectral range, the photocatalytic activity of TNT layers + 5c MoS_2 is enhanced and it is higher than that of TNT layers + 1c MoS_2. Indeed, in the VIS spectral region, MoS_2 is predominantly responsible for photodegradation due to its lower band gap compared to TiO_2. Diffuse reflectance UV-VIS spectra and the corresponding Kubelka–Munk curves (ESI, Fig. S7†) were recorded to determine the optical band gap energy of blank and MoS_2 decorated TNT layers. Values of ~3.12 eV, ~1.35 eV, and ~1.19 eV for blank TNT layers, TNT layers + 1c MoS_2, and TNT layers + 2c MoS_2 were determined, respectively. The difference in the band gap energy can be described as follows. One ALD cycle results into one S–Mo–S stack. Therefore, with an increased number of ALD cycles, the number of S–Mo–S stacks also increases. As the band gap energy of MoS_2 is strongly influenced by the number of S–Mo–S stacks, it will decrease with an increased number of these stacks. This suggests that the presence of MoS_2 on the surface of TiO_2 leads to the change in the electronic structure of TiO_2. It is apparent that TNT layers decorated by 1 or 2 ALD cycles of MoS_2 possess an increased incident light absorption. For the TNT layers + 5c MoS_2, it was not possible to measure any reflectivity, due to extremely black colour of the samples. Furthermore, the photocatalytic activity strongly depends on the quantity of the exposed edge sites of MoS_2.[18] An increase in the MoS_2 nanosheet thickness leads to smoothing its surface, thus decreasing the area of the exposed edge sites of MoS_2.[53] This is due to the non-ideal growth mode, which takes place, when layered materials such as MoS_2, are synthesized by thermal ALD[53] and also by the very nature of MoS_2 formation. Indeed, the active edge sites of MoS_2 and their formation were identified theoretically[54] and experimentally[55] for both crystalline[56] and amorphous[57] MoS_2. These previous reports and results shown herein confirm that TNT layers + 2c MoS_2 (theoretically 2 S–Mo–S stacks) rendered the best photocatalytic performance in the liquid phase under both UV and VIS light irradiation, due to a higher amount of exposed edge sites compared to TNT layers + 1c MoS_2 and TNT layers + 5c MoS_2.

Gas phase photodegradation in Fig. 4 shows kinetics and the total hexane-to-CO_2 conversion achieved on the blank and

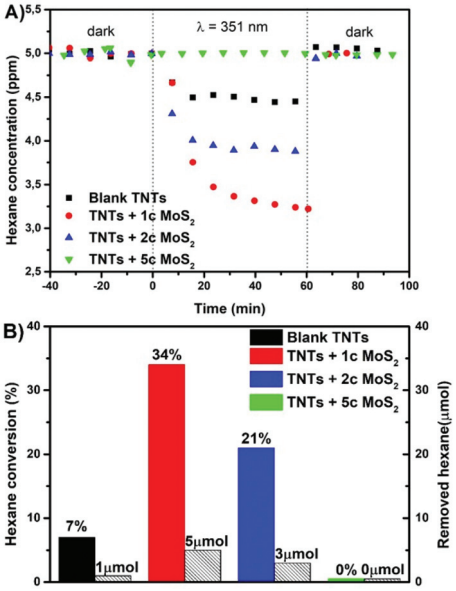

Fig. 4 Gas phase photocatalysis: (A) changes in the hexane concentration in the reactor upon UV light irradiation, (B) conversion and removal of hexane for blank and MoS_2 decorated TNT layers. The "*X*c" specifies the number of MoS_2 ALD cycles.

MoS_2 decorated TNT layers. The more detailed mechanism of hexane-to-CO_2 conversion is described in the ESI.† The highest photocatalytic conversion of hexane was achieved for 1 and 2 MoS_2 cycle decorated TNT layers with 34% and 21% conversion, removing the total of 5 μmol and 3 μmol of hexane which is ~5 and ~3 times higher compared to that of blank, respectively. The 5 MoS_2 cycle decoration of TNT layers did not show any measurable photoactivity.

By comparing Fig. 3 and 4, it is clear that the best photocatalytic activities in both the phases are obtained for different MoS_2 cycles (2c for the liquid and 1c for the gas phase). The reasons for this are not understood yet and require further investigation. However, while the difference in the homogeneity of the ALD MoS_2 nanosheets between the different nanotube layers used for the liquid and gas phase photocatalysis can be ruled out, the difference in the reactivity of the side edges of the MoS_2 nanosheets produced by 1c and 2c ALD cycles towards hexane degradation and diffusional and MoS_2 shading aspects of the different nanotube layers (with different morphological features) in general cannot be excluded.

Conclusions

In conclusion, the homogeneous decoration of TNT layers with MoS_2 nanosheets using ALD was demonstrated in this work. The ALD MoS_2 decorated TNT layers possess enhanced photocurrent densities with improved charge carrier transport and increased photocatalytic activities, in both phases (liquid and gas). The presented results clearly show how promising is the

combination of 1D supports with 2D materials. These results may also pave the way for more sophisticated devices and applications of these nanomaterial classes in future.

Conflicts of interest

There are no conflicts to declare.

Acknowledgements

The authors acknowledge the financial support from the European Research Council (ERC no. 638857) and the Ministry of Education, Youth and Sports of the Czech Republic (projects LM2015082, LO1411, LQ1601 and LTACH17007).

Notes and references

1 J. M. Macak, M. Zlamal, J. Krysa and P. Schmuki, *Small*, 2007, **3**, 300–304.
2 M. Zlamal, J. M. Macak, P. Schmuki and J. Krýsa, *Electrochem. Commun.*, 2007, **9**, 2822–2826.
3 I. Paramasivam, H. Jha, N. Liu and P. Schmuki, *Small*, 2012, **8**, 3073–3103.
4 H. Sopha, M. Krbal, S. Ng, J. Prikryl, R. Zazpe, F. K. Yam and J. M. Macak, *Appl. Mater. Today*, 2017, **9**, 104–110.
5 D. Regonini, G. Chen, C. Leach and F. J. Clemens, *Electrochim. Acta*, 2016, **213**, 31–36.
6 N. R. De Tacconi, C. R. Chenthamarakshan, G. Yogeeswaran, A. Watcharenwong, R. S. De Zoysa, N. A. Basit and K. Rajeshwar, *J. Phys. Chem. C*, 2006, **110**, 25347–25355.
7 L. Tsui, T. Homma and G. Zangari, *J. Phys. Chem. C*, 2013, **117**, 6979–6989.
8 J. M. Macák, H. Tsuchiya, A. Ghicov and P. Schmuki, *Electrochem. Commun.*, 2005, **7**, 1133–1137.
9 K. Zhu, N. R. Neale, A. Alexander Miedaner and A. J. Frank, *Nano Lett.*, 2007, **7**, 69–74.
10 A. L. Linsebigler, G. Lu and J. T. Yates, *Chem. Rev.*, 1995, **95**, 735–758.
11 M. R. Hoffmann, S. T. Martin, W. Choi, D. W. Bahnemann and W. M. Keck, *Chem. Rev.*, 1995, **95**, 69–96.
12 K. Rajeshwar, *J. Appl. Electrochem.*, 1995, **25**, 1067–1082.
13 Z. Li, X. Meng and Z. Zhang, *J. Photochem. Photobiol., C*, 2018, **35**, 39–55.
14 J. Theerthagiri, R. A. Senthil, B. Senthilkumar, A. Reddy Polu, J. Madhavan and M. Ashokkumar, *J. Solid State Chem.*, 2017, **252**, 43–71.
15 R. G. Dickinson and L. Pauling, *J. Am. Chem. Soc.*, 1923, **45**, 1466–1471.
16 X. Zhou, M. Lickleder and P. Schmuki, *Electrochem. Commun.*, 2016, **73**, 33–37.
17 D. Dumcenco, D. Ovchinnikov, K. Marinov, P. Lazi, M. Gibertini, N. Marzari, O. Lopez Sanchez, Y.-C. Kung, D. Krasnozhon, M.-W. Chen, S. Bertolazzi, P. Gillet, A. Fontcuberta Morral, A. Radenovic and A. Kis, *ACS Nano*, 2015, **9**, 4611–4620.
18 Y.-J. Yuan, H.-W. Lu, Z.-T. Yu and Z.-G. Zou, *ChemSusChem*, 2015, **8**, 4113–4127.
19 W. Zhou, Z. Yin, Y. Du, X. Huang, Z. Zeng, Z. Fan, H. Liu, J. Wang and H. Zhang, *Small*, 2013, **9**, 140–147.
20 Z. Xiong, L. L. Zhang and X. S. Zhao, *Chem. – Eur. J.*, 2011, **17**, 2428–2434.
21 S.-M. Lam, J.-C. Sin, A. Z. Abdullah and A. R. Mohamed, *J. Mol. Catal. A: Chem.*, 2013, **370**, 123–131.
22 M. Sabarinathan, S. Harish, J. Archana, M. Navaneethan, H. Ikeda and Y. Hayakawa, *RSC Adv.*, 2017, **7**, 24754–24763.
23 M. Mehta, A. P. Singh, S. Kumar, S. Krishnamurthy, B. Wickman and S. Basu, *Vacuum*, 2018, **155**, 675–681.
24 W. Teng, Y. Wang, H. Huang, X. Li and Y. Tang, *Appl. Surf. Sci.*, 2017, **425**, 507–517.
25 M. Sun, Y. Wang, Y. Fang, S. Sun and Z. Yu, *J. Alloys Compd.*, 2016, **684**, 335–341.
26 Y. Yu, J. Wan, Z. Yang and Z. Hu, *J. Colloid Interface Sci.*, 2017, **502**, 100–111.
27 H. N. T. Phung, V. N. K. Tran, L. T. Nguyen, L. K. T. Phan, P. A. Duong and H. V. T. Le, *J. Nanomater.*, 2017, **2017**, 1–6.
28 Y. Yu, S.-Y. Huang, Y. Li, S. N. Steinmann, W. Yang and L. Cao, *Nano Lett.*, 2014, **14**, 553–558.
29 D. Voiry, M. Salehi, R. Silva, T. Fujita, M. Chen, T. Asefa, V. B. Shenoy, G. Eda and M. Chhowalla, *Nano Lett.*, 2013, **13**, 6222–6227.
30 E. Parzinger, B. Miller, B. Blaschke, J. A. Garrido, J. W. Ager, A. Holleitner and U. Wurstbauer, *ACS Nano*, 2015, **9**, 11302–11309.
31 C. Meng, Z. Liu, T. Zhang and J. Zhai, *Green Chem.*, 2015, **17**, 2764–2768.
32 D. Wang, Y. Xu, F. Sun, Q. Zhang, P. Wang and X. Wang, *Appl. Surf. Sci.*, 2016, **377**, 221–227.
33 F. Dvorak, R. Zazpe, M. Krbal, H. Sopha, J. Prikryl, S. Ng, L. Hromadko, F. Bures and J. M. Macak, *Appl. Mater. Today*, 2019, **14**, 1–20.
34 M. Krbal, J. Prikryl, R. Zazpe, H. Sopha and J. M. Macak, *Nanoscale*, 2017, **9**, 7755–7759.
35 D. Voiry, M. Salehi, R. Silva, T. Fujita, M. Chen, T. Asefa, V. B. Shenoy, G. Eda and M. Chhowalla, *Nano Lett.*, 2013, **13**, 6222–6227.
36 Y.-J. Yuan, Z.-J. Ye, H.-W. Lu, B. Hu, Y.-H. Li, D.-Q. Chen, J.-S. Zhong, Z.-T. Yu and Z.-G. Zou, *ACS Catal.*, 2016, **6**, 532–541.
37 J. Liang, C. Wang, P. Zhao, Y. Wang, L. Ma, G. Zhu, Y. Hu, Z. Lu, Z. Xu, Y. Ma, T. Chen, Z. Tie, J. Liu and Z. Jin, *ACS Appl. Mater. Interfaces*, 2018, **10**, 6084–6089.
38 C. Liu, L. Wang, Y. Tang, S. Luo, Y. Liu, S. Zhang, Y. Zeng and Y. Xu, *Appl. Catal., B*, 2015, **164**, 1–9.
39 D. Wang, Y. Xu, F. Sun, Q. Zhang, P. Wang and X. Wang, *Appl. Surf. Sci.*, 2016, **377**, 221–227.
40 Y. Tian, Y. Song, M. Dou, J. Ji and F. Wang, *Appl. Surf. Sci.*, 2018, **433**, 197–205.
41 L. Yang, X. Zheng, M. Liu, S. Luo, Y. Luo and G. Li, *J. Hazard. Mater.*, 2017, **329**, 230–240.

42 L. Guo, Z. Yang, K. Marcus, Z. Li, B. Luo, L. Zhou, X. Wang, Y. Du and Y. Yang, *Energy Environ. Sci.*, 2018, **11**, 106–114.
43 H. Feng, N. Tang, S. Zhang, B. Liu and Q. Cai, *J. Colloid Interface Sci.*, 2017, **486**, 58–66.
44 L. Zheng, S. Han, H. Liu, P. Yu and X. Fang, *Small*, 2016, **12**, 1527–1536.
45 H. Sopha, A. Tesfaye, R. Zazpe, J. Michalicka, F. Dvorak, L. Hromadko, M. Krbal, J. Prikryl, T. Djenizian and J. M. Macak, *FlatChem*, 2019, **17**, 100130.
46 M. Motola, L. Satrapinskyy, T. Roch, J. Subrt, J. Kupcik, M. Klementova, M. Jakubickova, F. Peterka and G. Plesch, *Catal. Today*, 2017, **287**, 59–64.
47 H. Sopha, M. Baudys, M. Krbal, R. Zazpe, J. Prikryl, J. Krysa and J. M. Macak, *Electrochem. Commun.*, 2018, **97**, 91–95.
48 H. Li, Q. Zhang, C. C. R. Yap, B. K. Tay, T. H. T. Edwin, A. Olivier and D. Baillargeat, *Adv. Funct. Mater.*, 2012, **22**, 1385–1390.
49 L. Yang, C. Xie, J. Jin, R. Ali, C. Feng, P. Liu, B. Xiang, L. Yang, C. Xie, J. Jin, R. N. Ali, C. Feng, P. Liu and B. Xiang, *Nanomaterials*, 2018, **8**, 463.
50 A. Kuc, N. Zibouche and T. Heine, *Phys. Rev. B: Condens. Matter Mater. Phys.*, 2011, **83**, 245213.
51 Y.-J. Yuan, Z.-J. Ye, H.-W. Lu, B. Hu, Y.-H. Li, D.-Q. Chen, J.-S. Zhong, Z.-T. Yu and Z.-G. Zou, *ACS Catal.*, 2016, **6**, 532–541.
52 D. B. Nimbalkar, H.-H. Lo, P. V. R. K. Ramacharyulu and S.-C. Ke, *RSC Adv.*, 2016, **6**, 31661–31667.
53 T. A. Ho, C. Bae, S. Lee, M. Kim, J. M. Montero-Moreno, J. H. Park and H. Shin, *Chem. Mater.*, 2017, **29**, 7604–7614.
54 B. Hinnemann, P. G. Moses, J. Bonde, K. P. Jørgensen, J. H. Nielsen, S. Horch, A. I. Chorkendorff and J. K. Nørskov, *J. Am. Chem. Soc.*, 2005, **127**, 5308–5309.
55 T. F. Jaramillo, K. P. Jørgensen, J. Bonde, J. H. Nielsen, S. Horch and I. Chorkendorff, *Science*, 2007, **317**, 100–102.
56 J. Bonde, P. G. Moses, T. F. Jaramillo, J. K. Nørskov and I. Chorkendorff, *Faraday Discuss.*, 2009, **140**, 219–231.
57 C. G. Morales-Guio and X. Hu, *Acc. Chem. Res.*, 2014, **47**, 2671–2681.